Langerhans islets induce anti-tumor immunity at the expense of glycemic control and predict chemotherapy response in pancreatic cancer

Azaz Ahmed[1,2], Pornpimol Charoentong[1,3], Rosa Klotz[4], Sophia Köhler[1], Meggy Suarez-Carmona[2], Nektarios A. Valous[3], Dyke Ferber[1], Mathias Heikenwälder[5], Nathalia Giese[4], Thilo Hackert[4], Fee Klupp[4], Martin Schneider[4], Thomas Schmidt[4], Christoph Springfeld[1], Yakup Tanriver[6,7], Christine S. Falk[8], Laurence Zitvogel[9,10], Inka Zörnig[1,3], Dirk Jäger[1,3], Niels Halama[1,2]

[1] Medical Oncology and Internal Medicine VI, National Center for Tumor Diseases (NCT), University Hospital Heidelberg, University Heidelberg, 69120 Heidelberg, Germany

[2] Translational Immunotherapy, German Cancer Research Center (DKFZ), 69120 Heidelberg, Germany

[3] Applied Tumor Immunity Clinical Cooperation Unit, National Center for Tumor Diseases (NCT), German Cancer Research Center (DKFZ), 69120 Heidelberg, Germany

[4] General, Visceral and Transplantation Surgery, University Hospital Heidelberg, University Heidelberg, 69120 Heidelberg, Germany

[5] Chronic Inflammation and Cancer, German Cancer Research Center (DKFZ), 69120 Heidelberg, Germany

[6] Medical Microbiology and Hygiene, University of Freiburg, 79106 Freiburg, Germany

[7] Nephrology, Medical Center-University of Freiburg, 79106 Freiburg, Germany

[8] Institute of Transplant Immunology, Hannover Medical School, 30625 Hannover, Germany

[9] Université Paris XI, 91190 Saint-Aubin, France

[10] INSERM U1015, Institut Gustave Roussy, 94800 Villejuif, France

Correspondence to:

Niels Halama, MD

Translational Immunotherapy
German Cancer Research Center (DKFZ)
Im Neuenheimer Feld 242
69120 Heidelberg, Germany
phone: +49 6221 5638397
fax: + 49 6221 567030
email: niels.halama@nct-heidelberg.de

ABSTRACT

Induction of anti-tumor immunity in pancreatic ductal adenocarcinoma (PDA) is an unresolved challenge. Systematic investigation of the microenvironment of primary pancreatic tumors revealed a role of endocrine Langerhans islets in the coordination of immune activation. We found that intratumoral β-cells, regulated via STAT3, secrete C-C motif chemokine ligand 27 (CCL27) and thereby promote a T_H1 phenotype in the microenvironment resulting in an enhanced T cell infiltration and prolonged patient survival. The local effect can be abrogated in a patient-based human explant model by inhibition of the CCL27 receptor CCR10. This defense mechanism is paralleled by an impaired metabolic function of Langerhans islets with reduced insulin levels resulting in a dysregulation of glycemic control in patients. Based on these findings, screening of PDA cases (n= 2264) led to the identification of type 2 diabetes mellitus (T2DM) and extractable glycated haemoglobin (HbA1c) levels as response markers for neoadjuvant chemotherapy with fluorouracil, leucovorin, irinotecan and oxaliplatin (FOLFIRINOX). Collectively these data provide insights into the interconnection of T2DM and PDA, and link declining glycemic control to therapeutic efficacy, which can be utilized as a tool for clinical decision-making and improve patient management.

INTRODUCTION

Pancreatic ductal adenocarcinoma (PDA) is the seventh-leading cause of cancer-related death worldwide, with a 5-year survival of only 9% and the highest incidence-to-mortality ratio of any solid cancer[1]. Over the past decade, not only has the involvement of immune system in malignancies emerged as a critical hallmark of cancer[2], but immunotherapy has also profoundly changed cancer treatment by improving survival of patients in multiple solid tumors. A major predictor of clinical response to immunotherapy is the extent of intratumoral T cell infiltration. However, such “hot” tumors (high T cell infiltration) stand in contrast to “cold” tumors (low T cell infiltration) like PDA, which remains mostly refractory to immunotherapeutic treatment regimens[3]. A main feature of the tumor tissue in PDA is its desmoplastic microenvironment, in which immune cells make up nearly 50% of the cellular components but only few of them are anti-tumor effector cells such as $CD8^+$ T lymphocytes[4]. Human studies have shown that paucity of T cells is common in PDA, but a subset of primary tumors do exhibit moderate infiltration of $CD4^+$ or $CD8^+$ T cells, and their sheer presence correlates with expression of cytotoxicity genes and overall survival[5-8]. Induction of such an anti-tumor immunity can be induced, for example, by chemotherapy with fluorouracil, leucovorin, irinotecan and oxaliplatin (FOLFIRINOX) by increasing cytotoxic T cell densities. To further improve patient outcomes, we need to understand the role of the components defining the tumor microenvironment and identify critical immunomodulatory mechanisms[9-11].

In this regard, little is known about the role of endocrine Langerhans islets in shaping the tumoral immune landscape. Previous studies describe multiple proinflammatory cytokines originating from Langerhans islets in metabolic disorders such as obesity and diabetes[12,13]. Also, Langerhans islets are mainly responsible for chemokine-mediated inflammation and T cell infiltration in type 1 diabetes mellitus[14] and evidence suggests that this patient cohort is protected against PDA[15]. But what phenotype do Langerhans islets exhibit in the immune contexture of PDA? And is it clinically relevant? In addition, an impaired glycemic control is a common finding and several studies have shown a high incidence of type 2 diabetes mellitus (T2DM) in PDA patients[16] but it remains unclear whether T2DM is a risk factor or early marker of the disease[17-19].

This study aimed to systematically assess the tumor microenvironment and subsequently decipher immunologic interactions in PDA patients. This led to the in-depth investigation of anti-tumoral immunomodulatory capacities of Langerhans islets, their consequences for glycemic control and their impact on clinical outcomes, in order to tailor therapeutic strategies by exploiting metabolic parameters as a stratification marker.

MATERIAL AND METHODS

Patient samples and clinical analyses

All patients underwent planned surgery at the department for General, Visceral and Transplantation Surgery at the University Hospital Heidelberg. The study was approved by the local ethics committee (301/2001 and S-457/2019). Written informed consent was obtained from all patients. Tissue samples of 61 PDA patients were used for immunohistochemistry and cytokine analyses. 9 fresh PDA tissues on ice were directly collected from the operating room from patients who underwent surgery in 2019 and 2020. Survival analyses were performed on a set of 51 patients with PDA. Clinical information about diagnosis of T2DM, HbA1c levels and neoadjuvant treatment with FOLFIRNOX was collected in a cohort of 2264 patients, which is the total number of patients which was planned for pancreatoduodenectomy from 2016-2020 in the University Hospital Heidelberg. 122 patients were included in the final analysis. All patient data and samples were collected in a prospective database and analyzed retrospectively. All patient data was pseudonymized.

Patient-based organotypic tumor explant model

The organotypic tumor explant model was set up as previously described[20]. In brief, resected specimens were transferred on ice and under sterile conditions from the operating room to the laboratory. The timeframe was less than thirty minutes upon resection. The resected specimen was immediately processed into serial explant-suitable thin tissue sections (size approximately 6 x 6 x 1 mm). From each patient, one or more samples were directly frozen as well as formalin-fixed and embedded in paraffin for reference purposes. Tissue culture was performed by placing two explants with 1 ml of Minimum Essential Medium with 1% GlutaMAX supplement (Gibco, USA; 41090-036) per well on a 24-well plate in an incubator at 37°C and 5% CO_2. The explants were treated with a small molecule inhibitor of CCR10 (BI-6901) from (Boehringer Ingelheim, Germany). The CCR10 antagonist dosage per well was 0.1 mg/ml. Along with untreated explants (reference), the treated specimens were harvested after 24 hours and cryo-preserved using cryo embedding medium (Medite, USA; 41-3011-00) as well as formalin-fixed and embedded in paraffin.

Cell Culture of human pancreatic Langerhans islets

Human pancreatic Langerhans islet cells were purchased from (Celprogen, USA; 35002-04). The cells were seeded at 80% of confluence and plated at 10^5 per ml density. The cells were maintained in the appropriate size, extra-cellular matrix precoated flasks (Celprogen, USA; 35002-04-T75) and cultured in complete growth medium with serum (Celprogen, USA; M35002-04S). Medium was changed every 24 hours. When reached 65-75% of confluence, cells were passaged with 0,05% Trypsin-EDTA (Gibco, USA; 25300-054) and subcultured for expansion. Langerhans islet cells from passages 3 to 5 were used for the experiments.

Immunohistochemistry on human tissue samples

PDA tissue samples were collected freshly from the operating room, fixed in 4% phosphate buffered formaldehyde (ROTI Histofix, Roth, Germany; P087), placed in ethanol and embedded in paraffin. Tissue samples were sliced in 3 µm thick sections. All immunohistochemical stainings were performed on a BOND-MAX (Leica, Germany). FFPE tissues were deparaffinized and rehydrated (BOND Dewax Solution, Leica, Germany; AR9222). After heat-induced epitope retrieval (HIER) at 100°C (BOND Epitope Retrieval Solution 1 or 2, Leica, Germany; HIER 1 AR9961, HIER 2 AR9640), endogenous peroxidase activity was blocked by incubation with 3% peroxide block for 20 minutes (BOND Polymer Refine Detection System, Leica, Germany; DS9800). The sections were blocked with 10% normal goat serum (Vector, USA; S-1000-20). The primary antibodies were applied at room temperature for 30 minutes: CD3 (1:100, HIER 1, rabbit monoclonal, clone SP7, Abcam, UK; ab16669), CD4 (1:100, HIER 1, mouse monoclonal, clone 4B12, Leica, Germany; CD4-368-L-CE-H), CD8 (1:50, HIER 1, mouse monoclonal, clone 4B11, Leica, Germany, CD8-4B11-L-CE), CD20 (1:100, HIER 1, mouse monoclonal, clone L26, Leica, Germany; CD20-L26-L-CE), CD163 (1:500, HIER 2, rabbit monoclonal, clone EPR19518, Abcam, UK; ab182422), NKp46 (1:175, HIER 1, monoclonal mouse, clone 195314, R&D Systems, USA; MAB1850-500), FoxP3 (1:100, HIER 2, mouse monoclonal, clone 236A/E7, Thermo Fisher Scientific, Germany; 14-4777), CCL27 (1:200, HIER 1, mouse monoclonal, clone 124308, R&D Systems, USA; MAB376), CCR10 (1:100, HIER 1, rabbit polyclonal, Novus Biologicals, USA; NB100-56319), CA19-9 (1:1000, HIER 1, mouse monoclonal, clone 121SLE, Abcam, UK; ab3982), insulin (1:500000, rabbit monoclonal, clone EPR17359, Abcam, UK; ab181547), Phospho-Stat3 (Ser727) (1:200, HIER 2, mouse monoclonal, Cell Signaling Technology, USA; 9136S). The slides were incubated with a secondary antibody (rabbit anti-mouse IgG, BOND Polymer Refine Detection System, Leica, Germany, DS9800) for 8 minutes at room temperature. Signal amplification was performed by incubation with horse radish peroxidase and coupled to dextrane molecues in large numbers, for 8 minutes at room temperature (Poly-HRP-mouse anti-rabbit IgG, BOND Polymer Refine Detection System, Leica, Germany; DS9800). A color reaction with 3,3-di-amino-benzidine (DAB chromogen, BOND Polymer Refine Detection System; DS9800) was utilized to detect the antigen. Counterstaining was performed with haematoxylin (BOND Polymer Refine Detection System, Leica, Germany; DS9800) and the sections were mounted with Aquatex (Merck, Germany; 108562).

Immunofluorescence on human tissue samples

Immunofluorescence double staining was performed on paraffin-embedded sections using fluorochrome-conjugated secondary antibodies. For the first primary antibodies CD3, CD4, CD8 and FoxP3 a red fluorescence Alexa Fluor 594 donkey anti-mouse IgG (Thermo Fisher Scientific, Germany; A-21203) was used, and for CCR10 a green fluorescence Alexa 488 goat anti-rabbit IgG (Thermo Fisher Scientific, Germany; A-11008). For the analysis of the first primary antibody CCL27 and Phospho-Stat3 (Ser727) a green Alexa Fluor 488 goat anti-mouse IgG (Thermo Fisher Scientific, Germany; A-11029) was used, and for insulin a red Alexa Fluor 594 donkey anti-rabbit

IgG (Thermo Fisher Scientific, Germany; A-21207). The sections were stained according to antibody recommendation. After incubation of the first primary antibody overnight at 4°C, Alexa Fluor 488 (1:100 dilution) was applied for 60 minutes. The second primary antibody was applied for 180 minutes at room temperature and detected with Alexa Fluor 594 (1:100 dilution) for 60 minutes during sequential double staining. Mounting and staining for cell nuclei was performed using Vectashield with DAPI (1:10000, Vector, USA; H-1200). Images were taken with a Nanozoomer 2.0-HT slide scanner (Hamamatsu, Japan).

Whole-slide immune cell quantification

For quantification analysis of immune cells, tissue sections were digitized with a Leica Aperio AT2 scanner (Leica, Germany). Whole-slide microscopic images of full tissue sections were automatically obtained (virtual microscopy). The slides were scanned at 40-fold magnification and further examined using an image analysis software (VIS software suite, Visiopharm, Denmark). Given regions of interests (tumor and stroma) were manually annotated and density and distribution of immune cells was analyzed semi-automatically, as reported previously[21-23]. A visual consistency check was performed on all evaluations.

Laser capture microdissection

The tumoral and stromal compartment on PDA tissue sections was separated from each other by laser capture microdissection. This technique permits to isolate selected human cell populations from a section of complex tissue under direct microscopic visualization. The standard protocols of the inventers were used[24]. In brief, the tissue section was focused (20-fold magnification) and the tumoral and stromal area was manually separated using the Leica Laser Microdissection Software (Leica, Germany); the dissection was completed using a carbon dioxide laser pulse.

Multiplex protein quantification of cytokines and metabolic hormones

Small pieces of dissected frozen pancreatic tumor tissues were collected and lysed (Bio-Plex Cell Lysis Kit, BioRad, USA; 171304011), followed by a repeated procedure of vortexing, freezing (-80°C for 10 minutes), thawing (on ice) and ultrasonic bathing (for 10 minutes). The supernatants were then centrifuged at 13.000 rpm for 20 minutes at 4°C. When supernatants of cell culture experiments were analyzed no lysis was performed. In all samples, the protein concentrations were determined (Pierce BCA Protein Assay, Thermo Fisher Scientific, Germany; 23227), the concentration then was adjusted to 200 µg/ml and cytokine as well as metabolic hormone concentrations were quantified by multiplex protein arrays, according to the instructions of the manufacturer (BioRad, USA). A two-laser array reader simultaneously quantifies all proteins of interest (cytokines/metabolic hormones) and concentrations are calculated with Bio-Plex Manager 4.1.1 based on a 5-parameter logistic plot regression formula. For cytokine quantification Bio-Plex Pro Human Cytokine Screening Panel 48-plex (BioRad, USA; 12007283), Bio-Plex Pro Human Cytokine ICAM-1 (BioRad, USA; 171B6009M) and Bio-Plex Pro Human Cytokine VCAM-1

(BioRad, USA; 171B6022M) were used. For the quantification of metabolic hormones Bio-Plex Pro Human Diabetes 10-plex Assay (BioRad, USA; 171A7001M) was used. Previous experimental insights showed the technical reproducibility of this protocol [20].

Human Langerhans islets in tumoral microenvironment

Langerhans islets cells were placed in a 96-well plate (around 7500 cells/ per well) and cultured in a mixture of 150 µl volume of complete growth medium with serum (Celprogen, USA; M35002-04S) and 50 µl of supernatant of human PDA tissue explants. For reference purposes Langerhans islets cells were cultured in 200 µl of complete growth medium only. The supernatants were used to mimic a PDA tumor microenvironment and to investigate the behavior of intratumoral Langerhans islet cells. Supernatants of explants from five different PDA patients were used. The cells were treated for 48 hours. Afterwards, the total supernatants of the treated cells were collected and analyzed (Multiplex protein quantification of cytokines and metabolic hormones). For reference purposes the supernatant of undiluted human PDA tissue explants was also analyzed. The remaining cells were lysed (Bio-Plex Cell Lysis Kit, BioRad, USA; 171304011). In brief, the well-plate was placed on ice, the cells were rinsed with cell wash buffer and 120 µl of cell lysis buffer was added. The cells were incubated for 25 minutes on ice and during this time vortexed thoroughly every 5 minutes. After centrifugation (13.000 rpm for 30 minutes at 4°C), supernatant was collected and used for further analyses (signaling pathway analysis).

Signaling pathway analysis

Protein concentrations of lysate samples were determined (Pierce BCA Protein Assay, Thermo Fisher Scientific, Germany; 23227), the concentration then was adjusted from 20 to 130 µg/ml. Afterwards, multiple phosphorylated and total proteins were simultaneously quantified in each well of 96-well plates, using a protein array system according to the instructions of the manufacturer (BioRad, USA). A dual-laser microplate reader system detects the fluorescence of the individual dyed beads and the signal intensity on the bead surface. The relative abundance of each target protein is reported as the ratio of fluorescence among the wells. In the present study, Bio-Plex Pro Cell Signaling MAPK Panel 9-plex (BioRad, USA; LQ00000S6KL81S) and Bio-Plex Pro Cell Signaling Akt Panel 8-plex (BioRad, USA; LQ00006JK0K0RR) were used for phosphorylated protein quantification and Bio-Plex Pro Total Akt (BioRad, USA, 171V60001M), Bio-Plex Pro Total ERK1/2 (BioRad, USA, 171V60003M), Bio-Plex Pro Total GSK-3β (BioRad, USA, 171V60004M), Bio-Plex Pro Total JNK (BioRad, USA, 171V60007M), Bio-Plex Pro Total MEK1 (BioRad, USA, 171V60008M), Bio-Plex Pro Total PTEN (BioRad, USA, 171V60016M), Bio-Plex Pro Total mTOR (BioRad, USA, 171V60015M), Bio-Plex Pro Total p38 MAPK (BioRad, USA, 171V60009M), Bio-Plex Pro Total p70 S6 Kinase (BioRad, USA, 171V60010M), Bio-Plex Pro Total Human GAPDH (BioRad, USA, 171V60019M), Bio-Plex Pro Total β-Actin (BioRad, USA, 171V60001M) were used for quantification of total proteins. The protein concentrations are calculated with Bio-Plex Manager 4.1.1 based on a 5-parameter logistic plot regression formula.

246

247 **CCL27 quantification from stained tissue sections**

248 Samples were processed and stained automatically as described above. Whole-slide microscopic
249 images were obtained and calibrated for proper comparability as described previously [25].
250 Corresponding cytokine concentrations were used for reference and after calibration, tissues of
251 interest were quantified for CCL27 positivity and concentrations were calculated based on
252 reference curves.

253

254 **Statistics**

255 Normality of the distributions was tested with Shapiro-Wilk test, and for normal distributed data the
256 variance within each group of data was estimated and tested for equality between groups by a
257 two-sided F-test. Cytokines which were undetectable in more than 10 percentage of samples were
258 excluded. Correction for batch effects from three experiments was performed using the Python
259 package *pycombat* (version 0.14) and validated by analyzing the mixture of samples within UMAP
260 embeddings [26]. For comparison of two patient groups, two-sided Student's t test was used where
261 stated, otherwise the non-parametric two-sided Wilcoxon-rank sum test was used. Based on the
262 cytokine concentration data we reconstructed a T_H1 cytokine-cytokine co-expression network. The
263 edge weights of the network are based on the Pearson correlation coefficient between cytokine-
264 cytokine ($r \geq 0$, $P < 0.05$). Association of CCL27 concentrations with number of chemotherapy
265 cycles was done using Kendall rank correlation. Resulting p-values were adjusted for multiple
266 hypothesis testing according to the Benjamini and Hochberg method [27].
267 The overall survival time was defined using the latest information. For survival analysis, the
268 patients were dichotomized based on cytokine concentration and cell density. The median
269 cutpoints were determined to stratify patient into two groups (Hi and Lo). Kaplan Meier estimators
270 of survival were used to visualize the survival curves. The log-rank test was used to compare
271 overall survival between patients in different groups. P-values for the HiHi, HiLo, LoHi, and LoLo
272 cytokine/cell combination analysis were corrected for multiple testing using the Benjamini-
273 Hochberg method. All analyses were performed using the statistical software environment R
274 (package *survival*). Stated percentages and quartiles include rounded numbers. Statistical
275 analyses were carried out using R-4.0.2 and Python-3.6.4. Clustering and visualization were done
276 with the software Genesis [28].

RESULTS

Intratumoral CCL27 expression is associated with improved overall survival

To investigate the quantities of intratumoral immune cells and corresponding cytokine levels in PDA, we systematically performed stainings for $CD3^+$ T cells, $CD8^+$ T cells, $CD4^+$ T cells, $FoxP3^+$ T cells, $CD20^+$ B cells, $NKp46^+$ natural killer cells and $CD163^+$ tumor-associated macrophages and evaluated the expression profile of intratumoral cytokines in the resected tumor tissue of 51 PDA patients **(Table S1) (Figure S1A)**. These parameters were analyzed in relation to the clinical outcome of patients.

In tumor tissue, the only cytokine significantly associated with prolonged survival was the expression of C-C motif chemokine ligand 27 (CCL27) **(Figure 1A and 1B)**. Along with that, the tumor infiltration by $CD8^+$ cytotoxic T lymphocytes and the intratumoral $CD8^+/CD163^+$-ratio was significantly associated with improved survival **(Figure 1B)**. Particularly, the combination of intratumoral CCL27 and $CD8^+$ T cells proved to be a strong marker for favorable prognosis **(Figure 1B) (Table 1)**. On the other hand, intratumoral expression of IFN-γ was significantly associated with poorer survival in patients **(Figure 1A)**. The other intratumoral cytokines and immune cells tested were not significantly associated with overall survival **(Figure 1A)**. The association of clinical features (lymph node status, metastatic status, tumor grading) to overall survival confirmed previous reports **(Figure S1B)**.

β-cells within Langerhans islets are the source of CCL27 and its expression is correlated with a T_H1-type cytokine program

To elucidate whether the intratumoral expression of CCL27 relates to an immunity-driven anti-tumor signature within the tissue of PDA patients, we performed cytokine-cytokine correlation analyses. By that, we observed a characteristic T_H1-type cytokine signature correlating to the intratumoral presence of CCL27 **(Figure 2A and 2B)**.

Next, immunohistochemical and immunofluorescence stainings were performed on patient samples to identify the origin of CCL27 production. A staining for CCL27 revealed that islet-like structures within the tumor core are the main site of CCL27 expression **(Figure 2C)**. This observation prompted us to perform an immunofluorescence staining for the Langerhans islet marker insulin and CCL27, which corroborated that CCL27 is mainly expressed by β-cells within Langerhans islets **(Figure 2D)**.

CCR10 is expressed on $CD4^+$ $FoxP3^-$ T cells and selective inhibition of CCR10 abrogates the T_H1-type cytokine profile

Interaction of CCL27 with its only known receptor C-C chemokine receptor 10 (CCR10) is a key regulator for T-cell migration to the skin in inflammatory disorders[29]. And since our data revealed that tumor infiltration by cytotoxic T cells is independently prognostic favorable, we hypothesized that CCL27 might have similar immunomodulatory capacities in PDA. To identify CCR10-expressing cells in PDA, we performed systematic immunofluorescence stainings on patient

samples for $CCR10^+$ $CD3^+$ T cells, $CCR10^+$ $CD4^+$ T cells, $CCR10^+$ $FoxP3^+$ T cells and $CCR10^+$ $CD8^+$ T cells. A strong co-positivity for CCR10 was observed on $CD3^+$ and $CD4^+$ T cells **(Figure 3A)**. $FoxP3^+$ and $CD8^+$ T cells showed negligible expression of CCR10 **(Figure 3A)**.

To assess whether blockade of CCR10 abolishes anti-tumor properties in the microenvironment of PDA, we investigated the effect of a selective small molecule inhibitor of CCR10 (BI-6901) in a patient-based organotypic tumor explant model[20] **(Table S2) (Figure 3B)**. Inhibition of CCR10 led to an abrogation of the T_H1-type cytokine program by downregulating the expression of IFN-γ, IFN-α2, TNF-α and TNF-β **(Figure 3C)**. Other T_H1-supporting cytokines (TRAIL, IL-12p40, IL-12p70, IL-2, IL-7, IL-10) showed the same alteration **(Figure S3A)**. At the cellular level no difference was observed in the quantity of $CD163^+$ or $CD4^+$ cells upon blockade of CCR10 **(Figure 3D)**. However, the two tissues with the highest absolute number of $CD4^+$ lymphocytes showed the clearest reduction in tumor-infiltrating cytotoxic T cells after CCR10 inhibition **(Figure 3D)**.

Intratumoral Langerhans islet cells secrete CCL27 via STAT3 regulation and simultaneously downregulate insulin production

We aimed to determine the metabolic implications for immunomodulatory CCL27-producing Langerhans islets, which are primarily attributed to the endocrine regulation of glycemic control. To evaluate clinically relevant metabolic features of Langerhans islets, we sought to compare the preoperative glycemic status (type 2 diabetes mellitus (T2DM) or no T2DM) of PDA patients based on their intratumoral CCL27 expression. This analysis unraveled that CCL27 expression is significantly associated with the onset of T2DM in tumor patients **(Figure 4A)**. Furthermore, the marker combination of CCL27 and preoperative diagnosis of diabetes was shown to serve as a potential parameter for favorable prognosis. However, T2DM is a complex disease with multiple negative implications for human health and further investigation is needed to better understand the role of different types of diabetes and the timepoint of disease onset (long-standing vs. new-onset T2DM) in the context of PDA **(Figure 4B) (Table 2)**.

To more fully characterize the multifaceted role of Langerhans islets in PDA, we explored their secretion and signaling profile after exerting tumoral stress on them **(Figure 4C)**. The tumor microenvironment for this analysis was mimicked by using the supernatant of PDA explants from five different patients. We observed that tumoral stress led to an increased secretion of CCL27 matching our previous findings **(Figure 4D)**. Simultaneously, the secretion of insulin and glucagon was downregulated **(Figure 4D)**. While on the other hand, the secretion of the incretin glucose-dependent insulinotropic polypeptide (GIP) as well as the production of the hormone resistin was increased in Langerhans islet cells **(Figure 4D)**. The same tendency (upregulation in 3 of 5 cases) was seen for glucagon-like peptide 1 (GLP-1) **(Figure S4A)**. However, evaluation of dynamic changes in hormone concentrations is necessary to comprehensively understand these regulatory mechanisms.

Molecular analyses based on protein phosphorylation patterns in these Langerhans islets cells showed an activation of signal transducer and activator of transcription 3 (STAT3) and BCL2-associated agonist of cell death (BAD) upstream regulated by phosphatase and tensin homologue (PTEN) and AKT (also known as protein kinase B or PKB). Simultaneously, the extracellular signal-regulated kinases 1 and 2 (ERK1/2) were dephosphorylated and thereby inactivated **(Figure 4E and S4B)**. Further, we corroborated the phosphorylation of STAT3 in intratumoral Langerhans islets via immunofluorescence staining by comparing human PDA tissue and healthy pancreas tissue **(Figure 4F)**.

T2DM and dynamic of HbA1c levels are markers for response to neoadjuvant chemotherapy

To explore the relationship of tumoral CCL27 expression and treatment response to adjuvant chemotherapy (= number of adjuvant chemotherapy cycles), we performed a comparison analysis between tissues of patients with high tumoral CCL27 expression ($CCL27^{hi}$) and low tumoral CCL27 expression ($CCL27^{lo}$). We discovered that CCL27 expression, also in a linear relationship, was significantly associated with the number of chemotherapy cycles **(Figure 5A)**.

Since CCL27 secretion is linked to glycemic control, we hypothesized that diagnosis of T2DM or glycated haemoglobin (HbA1c) levels may have the potential to identify patients who are most likely to respond to chemotherapy. To investigate this, we screened a cohort of 2264 PDA patients who were planned for pancreatoduodenectomy **(Figure B)**. We identified 122 patients who had undergone neoadjuvant chemotherapy with FOLFIRINOX prior to the planned surgery and with extractable data on HbA1c levels before and after FOLFIRINOX **(Table 3)**. The retrospective analysis unveiled that diagnosis of T2DM was significantly associated with response to neoadjuvant chemotherapy with FOLFIRINOX **(Figure 5B)**. Moreover, decline of glycemic control (= increase of HbA1c levels) during neoadjuvant chemotherapy with FOLFIRINOX was also significantly associated with treatment response. This observation was statistically significant in PDA patients with and without T2DM **(Figure S5A)**. In contrast, improved glycemic control (= decrease of HbA1c levels) was significantly associated with unresponsiveness to neoadjuvant FOLFIRINOX **(Figure 5 B)**. This was significant in patients without T2DM and the same trend was seen for patients with T2DM **(Figure S5A)**.

To confirm our concept that deterioration of glycemic control is accompanied by increased local CCL27 levels, we analyzed the tumor tissue of a patient who responded to neoadjuvant chemotherapy with FOLFIRINOX and had a rising HbA1c level **(Figure 5C)**. This case validated our findings and demonstrated that not only did the HbA1c level increase, but also the local CCL27 concentration **(Figure 5 C and S5B)**.

DISCUSSION

Induction of anti-tumor immunity by increasing the number of tumor-infiltrating T cells is an unresolved challenge and limited T cell infiltration is a major reason for resistance to immunotherapy in PDA. In the present report, we demonstrate a crucial role of endocrine Langerhans islets in shaping anti-tumor immunity by undergoing a phenotype shift from glycemic control to CCL27 production. Subsequently, CCL27 promotes a T_H1-type cytokine program in the microenvironment, enhances tumoral T cell infiltration and improves survival of patients. To date, CCL27 has primarily been described as a chemotactic mediator of T cell-dependent (skin) inflammation and previous reports showed concordantly that CCL27 induces T cell attraction and inflammation via $CCR10^+$ $CD4^+$ T lymphocytes whereas $CD8^+$ T lymphocytes show negligible levels of CCR10 on their cell surface[29,30]. Our data corroborated these findings in the context of PDA and demonstrated that the anti-tumor effect can be abrogated by inhibition of CCR10. In other malignancies CCL27-CCR10 interaction has been suspected to promote lymph node metastases[31] and contribute to inflammation-driven hepatocarcinogenesis[32]. However, our results highlight that CCL27-CCR10 interaction plays an opposite role in the microenvironment of PDA by potentially turning it into an immunologically “hot” tumor with beneficial clinical outcomes. Also, our data indicate that efficacy of effector T cell-attraction by CCL27 is dependent on the quantity of $CCR10^+$ $CD4^+$ T cells, in order to generate a sufficient T_H1-cytokine signal. This is line with existing evidence, which showed that $CD4^+$ T cells play a fundamental role in driving anti-tumor $CD8^+$ T cell responses and that their presence is associated with the number of $CD8^+$ T cells in solid tumors[33,34]. The use of a fully human patient-derived model in our experiments allowed us to link the clinical observations to functional molecular findings.

Another interesting aspect of our results is that endocrine Langerhans islet cells were identified as the primary source of CCL27 suggesting a critical involvement of the endocrine-exocrine axis in anti-tumor immunity. Primarily, Langerhans islets are attributed to the endocrine regulation of glycemic control, which requires a precisely fine-tuned balance of multiple glucoregulatory hormones. Glucose homeostasis is primarily regulated by a tug-of-war between endocrine Langerhans islet hormones. Glucagon is secreted by α-cells and increases plasma glucose levels, whereas insulin from β-cells decreases them. Furthermore, a variety of other hormones are critically involved, such as the incretins GIP and GLP-1, which are secreted by α-cells and regulate blood glucose levels through potentiation of insulin secretion and inhibition of glucagon secretion[35-39]. In light of the existing evidence, our findings suggest that while intratumoral β-cells secrete CCL27 which inhibits tumor progression, their metabolic function declines resulting in an insulin deficiency. This eventually leads to a compensatory upregulation of intrainsular GIP and GLP-1 secretion, which fail to properly potentiate insulin expression but inhibit glucagon secretion. This mechanism of endocrine-exocrine interaction also explains our clinical observation that onset of T2DM in PDA patients is significantly associated with CCL27 expression of tumors. In addition, the observed lower insulin levels might further help to limit

aberrant activation of oncogenic signaling pathways and may contribute to systemic antineoplastic functions[40-42]. Another factor potentially contributing to the loss of glycemic control in patients is the upregulated resistin secretion. Resistin is secreted by adipocytes and Langerhans islets, known as a key link between obesity and diabetes and leads to peripheral insulin resistance[43].

Further, the identification of STAT3 as activator of CCL27 production is in line with previous findings, which presented its common involvement in cytokine release by Langerhans islet cells[44]. Interestingly, STAT3 also plays a critical role in inhibiting insulin secretion in mice[45,46], which corroborates our findings. And the observed phosphorylation and activation of anti-apoptotic BAD might contribute to preservation of this CCL27-releasing and insulin-inhibiting phenotype of Langerhans islets.

The interplay of T2DM to PDA is complex and, despite numerous studies, not comprehensively understood. However, strong existing evidence demonstrated that (new-onset) T2DM is likely to be a consequence of a tumor microenvironment consisting of progressively growing PDA cells[47]. We complement prior findings by showing that onset of T2DM is a potential sign of functionally shifting Langerhans islets towards shaping anti-tumor immunity via CCL27 production as a defense mechanism against PDA. This observation also underscores the complex and bilateral role of local immunity in PDA: While IL-1β-induced pancreatitis promotes PDA via immunosuppression[48], development of T2DM promotes autoimmune anti-tumor responses via CCL27. Further, the interconnection of glycemic control and PDA prompted us to investigate metabolic parameters as markers for response to neoadjuvant chemotherapy with FOLFIRINOX. Historically, the combination therapies FOLFIRINOX and gemcitabine with nab-paclitaxel significantly increased survival of patients[49,50]. While FOLFIRINOX is more effective than gemcitabine, the regimen also causes more side effects and significantly reduces quality of life of patients. However, response to chemotherapy varies, with only one third of patients responding to a specific regimen[51]. Given the fact that patients with unresponsiveness to neoadjuvant chemotherapy and irresectable PDA have a median life expectancy of less than a year preventing FOLFIRINOX-induced toxicity is an urgent clinical need. FOLFIRINOX is known to induce an anti-tumor immune infiltrate in the pancreatic tumor microenvironment, which is characterized by increased cell densities of $CD8^+$ and $CD4^+$ T lymphocytes as well as decreased numbers of $FoxP3^+$ and $CD163^+$ cells[52-54]. We hypothesize that this local immune reaction is the reason for our observation of elevated HbA1c levels and increased CCL27 secretion after exposure to FOLFIRINOX, similarly to the production of inflammatory signals as an Langerhans islet response to various local inflammatory factors during development of diabetes[14,55,56]. Our findings highlight that the presence of T2DM before the start of neoadjuvant chemotherapy as well as the dynamic of HbA1c levels during the treatment are markers for response to FOLFIRINOX. In line with this, another independent clinical investigation demonstrated that elevated HbA1c levels can be utilized as a marker for stratifying patients most likely to respond to FOLFIRINOX[51].

In conclusion, our findings describe a novel mechanism of anti-tumor action in PDA unravelling an unexpected role for endocrine Langerhans islets with implications for the clinical

management of PDA. Repurposing metabolic parameters has the potential to serve as a tool for clinical decision-making. However, prospective clinical trials are needed to further investigate these applications. Also, CCL27-CCR10 interaction could serve as a stratification parameter for immunotherapeutic strategies.

ACKNOWLEDGEMENTS

We thank Jana Wolf, Ulrike Prüfer and Rosa Eurich for excellent technical assistance. Schematic figures were created with BioRender.com. PDA samples were provided by the Pancobank platform at the European Pancreas Center Heidelberg (EPZ), member of the Biomaterial Bank Heidelberg (BMBH).

CONTRIBUTORS

Conceptualization, A.A. and N.H.; Methodology, A.A., S.K., M.S. and N.H.; Formal Analysis, A.A., P.C., D.F. and N.H.; Investigation, A.A., S.K. and R.K.; Resources, R.K., T.H., N.G., M.H., C.S., C.F., I.Z., D.J. and N.H.; Data Curation, A.A., P.C. and N.H.; Writing - Original Draft, A.A.; Writing - Review & Editing, A.A, R.K., S.K., M.S, N.V., D.F., M.H., N.G., C.S., C.F., M.S., T.S., Y.T., L.Z., I.Z., D.J. and N.H.; Visualization, A.A., P.C., N.V. and N.H.; Supervision, I.Z., D.J. and N.H.; Project Administration, A.A. and N.H.; Funding Acquisition, I.Z., D.J. and N.H.

FUNDING

This study was supported by the RR Pohl Stiftung.

COMPETING INTERESTS

None declared.

ETHICS APPROVAL

Ethics Committee of the University of Heidelberg.

DATA AVAILABILITY STATEMENT

All data are available upon request. All data relevant to the study are included in the article or uploaded as supplementary information.

REFERENCES

1. Bray, F., *et al.* Global cancer statistics 2018: GLOBOCAN estimates of incidence and mortality worldwide for 36 cancers in 185 countries. *CA: a cancer journal for clinicians* **68**, 394-424 (2018).
2. Hanahan, D. & Weinberg, R.A. Hallmarks of cancer: the next generation. *cell* **144**, 646-674 (2011).
3. Sharma, P. & Allison, J.P. The future of immune checkpoint therapy. *Science* **348**, 56-61 (2015).
4. Clark, C.E., *et al.* Dynamics of the immune reaction to pancreatic cancer from inception to invasion. *Cancer research* **67**, 9518-9527 (2007).
5. Balachandran, V.P., *et al.* Identification of unique neoantigen qualities in long-term survivors of pancreatic cancer. *Nature* **551**, 512-516 (2017).
6. Bailey, P., *et al.* Genomic analyses identify molecular subtypes of pancreatic cancer. *Nature* **531**, 47-52 (2016).
7. Vonderheide, R.H. The immune revolution: a case for priming, not checkpoint. *Cancer cell* **33**, 563-569 (2018).
8. Wang, Z., Zhao, J. & Zhao, H. Infiltrating CD4/CD8 high T cells shows good prognostic impact in pancreatic cancer. *International Journal of Clinical and Experimental Pathology* **10**, 8820 (2017).
9. Buck, M.D., Sowell, R.T., Kaech, S.M. & Pearce, E.L. Metabolic instruction of immunity. *Cell* **169**, 570-586 (2017).
10. Foley, K., Kim, V., Jaffee, E. & Zheng, L. Current progress in immunotherapy for pancreatic cancer. *Cancer letters* **381**, 244-251 (2016).
11. Ho, W.J., Jaffee, E.M. & Zheng, L. The tumor microenvironment in pancreatic cancer—clinical challenges and opportunities. *Nature Reviews Clinical Oncology*, 1-14 (2020).
12. Weisberg, S.P., *et al.* CCR2 modulates inflammatory and metabolic effects of high-fat feeding. *The Journal of clinical investigation* **116**, 115-124 (2006).
13. Ying, W., *et al.* Expansion of islet-resident macrophages leads to inflammation affecting β cell proliferation and function in obesity. *Cell metabolism* **29**, 457-474. e455 (2019).
14. Frigerio, S., *et al.* β cells are responsible for CXCR3-mediated T-cell infiltration in insulitis. *Nature medicine* **8**, 1414-1420 (2002).
15. Hennig, R., Ding, X. & Adrian, T.E. On the role of the islets of Langerhans in pancreatic cancer. *Histology and histopathology* (2004).
16. De Souza, A., Irfan, K., Masud, F. & Saif, M.W. Diabetes type 2 and pancreatic cancer: a history unfolding. *JOP: Journal of the pancreas* **17**, 144 (2016).
17. Busaidy, N., *et al.* Survival of resectable pancreatic cancer patients with diabetes. *Journal of Clinical Oncology* **24**, 4098-4098 (2006).
18. Kang, S.P. & Saif, M.W. Clinical outcome of pancreatic cancer patients with diabetes mellitus: is diabetes a poor prognostic factor? *JOP. Journal of the Pancreas* **11**, 334-335 (2010).
19. Gullo, L., Pezzilli, R., Morselli-Labate, A.M. & Group, I.P.C.S. Diabetes and the risk of pancreatic cancer. *New England Journal of Medicine* **331**, 81-84 (1994).
20. Halama, N., *et al.* Tumoral immune cell exploitation in colorectal cancer metastases can be targeted effectively by anti-CCR5 therapy in cancer patients. *Cancer cell* **29**, 587-601 (2016).
21. Halama, N., *et al.* Estimation of immune cell densities in immune cell conglomerates: an approach for high-throughput quantification. **4**, e7847 (2009).
22. Halama, N., *et al.* Quantification of prognostic immune cell markers in colorectal cancer using whole slide imaging tumor maps. **32**, 333-340 (2010).
23. Halama, N., *et al.* Natural killer cells are scarce in colorectal carcinoma tissue despite high levels of chemokines and cytokines. **17**, 678-689 (2011).

24. Emmert-Buck, M.R., *et al.* Laser capture microdissection. **274**, 998-1001 (1996).
25. Inman, C., *et al.* Validation of computer-assisted, pixel-based analysis of multiple-colour immunofluorescence histology. *Journal of immunological methods* **302**, 156-167 (2005).
26. McInnes, L., Healy, J. & Melville, J. Umap: Uniform manifold approximation and projection for dimension reduction. *arXiv preprint arXiv:1802.03426* (2018).
27. Benjamini, Y. & Hochberg, Y. Controlling the false discovery rate: a practical and powerful approach to multiple testing. *Journal of the Royal statistical society: series B (Methodological)* **57**, 289-300 (1995).
28. Sturn, A., Quackenbush, J. & Trajanoski, Z. Genesis: cluster analysis of microarray data. *Bioinformatics* **18**, 207-208 (2002).
29. Homey, B., *et al.* CCL27–CCR10 interactions regulate T cell–mediated skin inflammation. *Nature medicine* **8**, 157-165 (2002).
30. Wang, X., *et al.* Visualizing CD4 T-cell migration into inflamed skin and its inhibition by CCR4/CCR10 blockades using in vivo imaging model. *British Journal of Dermatology* **162**, 487-496 (2010).
31. Karnezis, T., *et al.* CCL27/CCL28–CCR10 Chemokine Signaling Mediates Migration of Lymphatic Endothelial Cells. *Cancer Research* **79**, 1558-1572 (2019).
32. Wu, Q., *et al.* The chemokine receptor CCR10 promotes inflammation-driven hepatocarcinogenesis via PI3K/Akt pathway activation. *Cell Death & Disease* **9**, 1-18 (2018).
33. Tay, R.E., Richardson, E.K. & Toh, H.C. Revisiting the role of CD4+ T cells in cancer immunotherapy—new insights into old paradigms. *Cancer Gene Therapy*, 1-13 (2020).
34. Zander, R., *et al.* CD4+ T cell help is required for the formation of a cytolytic CD8+ T cell subset that protects against chronic infection and cancer. *Immunity* **51**, 1028-1042. e1024 (2019).
35. Dupre, J., Ross, S., Watson, D. & Brown, J. Stimulation of insulin secretion by gastric inhibitory polypeptide in man. *The Journal of Clinical Endocrinology & Metabolism* **37**, 826-828 (1973).
36. Kreymann, B., Ghatei, M., Williams, G. & Bloom, S. Glucagon-like peptide-1 7-36: a physiological incretin in man. *The Lancet* **330**, 1300-1304 (1987).
37. Mojsov, S., Weir, G. & Habener, J. Insulinotropin: glucagon-like peptide I (7-37) co-encoded in the glucagon gene is a potent stimulator of insulin release in the perfused rat pancreas. *The Journal of clinical investigation* **79**, 616-619 (1987).
38. Fujita, Y., *et al.* Glucose-dependent insulinotropic polypeptide is expressed in pancreatic islet α-cells and promotes insulin secretion. *Gastroenterology* **138**, 1966-1975. e1961 (2010).
39. Komatsu, R., *et al.* Glucagonostatic and insulinotropic action of glucagonlike peptide I-(7–36)-amide. *Diabetes* **38**, 902-905 (1989).
40. Tajan, M. & Vousden, K.H. Dietary Approaches to Cancer Therapy. *Cancer Cell* (2020).
41. Halbrook, C.J. & Lyssiotis, C.A. Employing metabolism to improve the diagnosis and treatment of pancreatic cancer. *Cancer cell* **31**, 5-19 (2017).
42. Trajkovic-Arsic, M., Kalideris, E. & Siveke, J.T. The role of insulin and IGF system in pancreatic cancer. *J Mol Endocrinol* **50**, R67-R74 (2013).
43. Steppan, C.M., *et al.* The hormone resistin links obesity to diabetes. *Nature* **409**, 307-312 (2001).
44. Cheng, Y., *et al.* Hypoxia/reoxygenation-induced HMGB1 translocation and release promotes islet proinflammatory cytokine production and early islet graft failure through TLRs signaling. *Biochimica et Biophysica Acta (BBA)-Molecular Basis of Disease* **1863**, 354-364 (2017).
45. Velayos, T., *et al.* An activating mutation in STAT3 results in neonatal diabetes through reduced insulin synthesis. *Diabetes* **66**, 1022-1029 (2017).

46. Chen, J.*, et al.* LIM-homeodomain transcription factor Isl-1 mediates the effect of leptin on insulin secretion in mice. *Journal of Biological Chemistry* **288**, 12395-12405 (2013).
47. Molina-Montes, E.*, et al.* Deciphering the complex interplay between pancreatic cancer, diabetes mellitus subtypes and obesity/BMI through causal inference and mediation analyses. *Gut* **70**, 319-329 (2021).
48. Takahashi, R.*, et al.* Interleukin-1β-induced pancreatitis promotes pancreatic ductal adenocarcinoma via B lymphocyte–mediated immune suppression. *Gut* **70**, 330-341 (2021).
49. Conroy, T.*, et al.* FOLFIRINOX versus gemcitabine for metastatic pancreatic cancer. *New England Journal of Medicine* **364**, 1817-1825 (2011).
50. Von Hoff, D.D.*, et al.* Increased survival in pancreatic cancer with nab-paclitaxel plus gemcitabine. *New England Journal of Medicine* **369**, 1691-1703 (2013).
51. Capello, M.*, et al.* CES2 Expression in Pancreatic Adenocarcinoma Is Predictive of Response to Irinotecan and Is Associated With Type 2 Diabetes. *JCO Precision Oncology* **4**, 426-436 (2020).
52. Cai, L.*, et al.* Enhancement of anti-tumor immunity and survival prolongation by neoadjuvant 5-FU, oxaliplatin and irinotecan (folfirinox) in pancreatic ductal adenocarcinoma patients. *HPB* **20**, S10 (2018).
53. Peng, H.*, et al.* Response to FOLFIRINOX neoadjuvant chemotherapy is associated with a high prevalence of Tbet expressing T cells in pancreatic cancer patients. (Am Assoc Immnol, 2020).
54. Michelakos, T.*, et al.* Tumor microenvironment immune response in pancreatic ductal adenocarcinoma patients treated with neoadjuvant therapy. *JNCI: Journal of the National Cancer Institute* (2020).
55. Arnush, M.*, et al.* IL-1 produced and released endogenously within human islets inhibits beta cell function. *The Journal of clinical investigation* **102**, 516-526 (1998).
56. Donath, M.Y.*, et al.* Islet inflammation in type 2 diabetes: from metabolic stress to therapy. *Diabetes care* **31**, S161-S164 (2008).

TABLES

Table 1. Subject characteristics

		$CCL27^{hi}$ $CD8^{hi}$	$CCL27^{lo}$ $CD8^{hi}$	$CCL27^{hi}$ $CD8^{lo}$	$CCL27^{lo}$ $CD8^{lo}$	P-value
Total number of patients (n)		16	9	9	16	
Female / Male (n / n)		11 / 5	3 / 6	5 / 4	5 / 11	0.143
Age	Mean (years)	67.8±0.6	68.6±1.3	63.8±0.9	61.8±0.7	
	> / ≤ Average age[a] (n / n)	11 / 5	5 / 4	4 / 5	8 / 8	0.634
BMI[b]	Mean (kg/m^2)	25.5±0.2	23.3±0.4	22.9±0.4	24.7±0.2	
	> / ≤ Average BMI[c] (n / n)	9 / 4	2 / 3	2 / 6	5 / 8	0.236
T	T3 (n)	16	9	9	15	1.000
	T4 (n)	0	0	0	1	
N	N0 (n)	3	2	2	1	0.689
	N1 (n)	13	7	7	15	
M	M0 (n)	15	9	8	15	1.000
	M1 (n)	1	0	1	1	
Grade	G2 (n)	10	8	3	10	0.184
	G3 (n)	6	1	5	6	
R[d]	R0 (n)	4	1	0	1	0.339
	R1 (n)	12	8	9	15	
Gemcitabine-based chemotherapy (n)[e]		15	5	6	9	
Diabetes prior to surgery (yes (n) / no (n))[f]		8 / 1	3 / 4	2 / 4	3 / 10	0.018
Overall survival (days)		919±41	596±39	606±43	319±13	

Data are shown as mean ± SEM.

Fisher's exact test was used to compare patients of the different groups.

T= stage of primary tumor, N= regional lymph node status, M= distant metastasis status, R= resection margin status, BMI= Body-Mass-Index.

[a] *Average age in all patients is 65.3 years.*

[b] *Information available on BMI from 39 patients.*

[c] *Average BMI in all patients is 24.43 kg/m^2.*

[d] *Information available on resection margin status from 50 patients.*

[e] *Standard treatment in the study period was upfront resection and gemcitabine-based adjuvant chemotherapy. Information available on confirmed application of gemcitabine from 35 patients.*

[f] *Information available on glycemic status (according to HbA1c levels or medical history) from 35 patients.*

Table 2. Subject characteristics

		CCL27^{hi} Diabetes	CCL27^{hi} No diabetes	CCL27^{lo} Diabetes	CCL27^{lo} No diabetes	P-value
Total number of patients (n)		10	5	6	14	
Female / Male (n / n)		8 / 2	3 / 2	1 / 5	4 / 10	0.033
Age	Mean (years)	68.9±0.9	62.2±1.7	65.7±1.7	61.8±0.9	
	> / ≤ Average age[a] (n / n)	8 / 2	2 / 3	3 / 3	7 / 7	0.353
BMI[b]	Mean (kg/m^2)	25.7±0.5	21.8±0.7	23.1±0.5	24.7±0.2	
	> / ≤ Average BMI[c] (n / n)	6 / 2	1 / 4	1 / 4	6 / 4	0.153
T	T3 (n)	10	5	6	13	1.000
	T4 (n)	0	0	0	1	
N	N0 (n)	3	0	0	2	0.503
	N1 (n)	7	5	6	12	
M	M0 (n)	10	5	6	13	1.000
	M1 (n)	0	0	0	1	
Grade	G2 (n)	6	2	5	9	0.592
	G3 (n)	4	3	1	5	
R[d]	R0 (n)	2	0	0	2	0.731
	R1 (n)	8	5	6	11	
HbA1c level[e]	Mean (%)	7.0±0.08	5.8±0.06	7.5±0.20	5.4±0.04	
	> / ≤ Average HbA1c[f] (n / n)	9 / 1	1 / 4	6 / 0	0 / 13	< 0.0001
Gemcitabine-based chemotherapy (n)[g]		10	4	3	10	
Overall survival (days)		849±52	843±106	450±60	370±17	

Data are shown as mean ± SEM.

Fisher's exact test was used to compare patients of the different groups.

T= stage of primary tumor, N= regional lymph node status, M= distant metastasis status, R= resection margin status, BMI= Body-Mass-Index.

[a] *Average age in all patients is 64.5 years.*

[b] *Information available on BMI from 28 patients.*

[c] *Average BMI in all patients is 24.18 kg/m^2.*

[d] *Information available on resection margin status from 34 patients.*

[e] *Information available on HbA1c level from 34 patients.*

[f] *Average HbA1c level in all patients is 6.3 %.*

[g] *Standard treatment in the study period was upfront resection and gemcitabine-based adjuvant chemotherapy. Information available on confirmed application of gemcitabine from 27 patients.*

Table 3. Subject characteristics

		Response to FOLFIRINOX		No response to FOLFIRINOX	
		T2DM	No T2DM	T2DM	No T2DM
Total number of patients (n)		38	37	11	36
Female / Male (n / n)		20 / 18	20 / 17	3 / 8	10 / 26
Age (years)		62.1±1.3	58.8±1.6	65.9±2.0	59.6±2.1
T	T1 (n)	8	12	Irresectable (no histopathology)	
	T2 (n)	13	16		
	T3 (n)	14	7		
	T4 (n)	3	2		
N	N0 (n)	16	20		
	N1 (n)	15	9		
	N2 (n)	7	8		
M	M0 (n)	34	33		
	M1 (n)	4	4		
R	R0 (n)	29	27		
	R1 (n)	9	10		

Data are shown as mean ± SEM.

T= stage of primary tumor, N= regional lymph node status, M= distant metastasis status, R= resection margin status.

FOLFIRINOX= fluorouracil, leucovorin, irinotecan and oxaliplatin

T2DM= type 2 diabetes mellitus

Figure 1

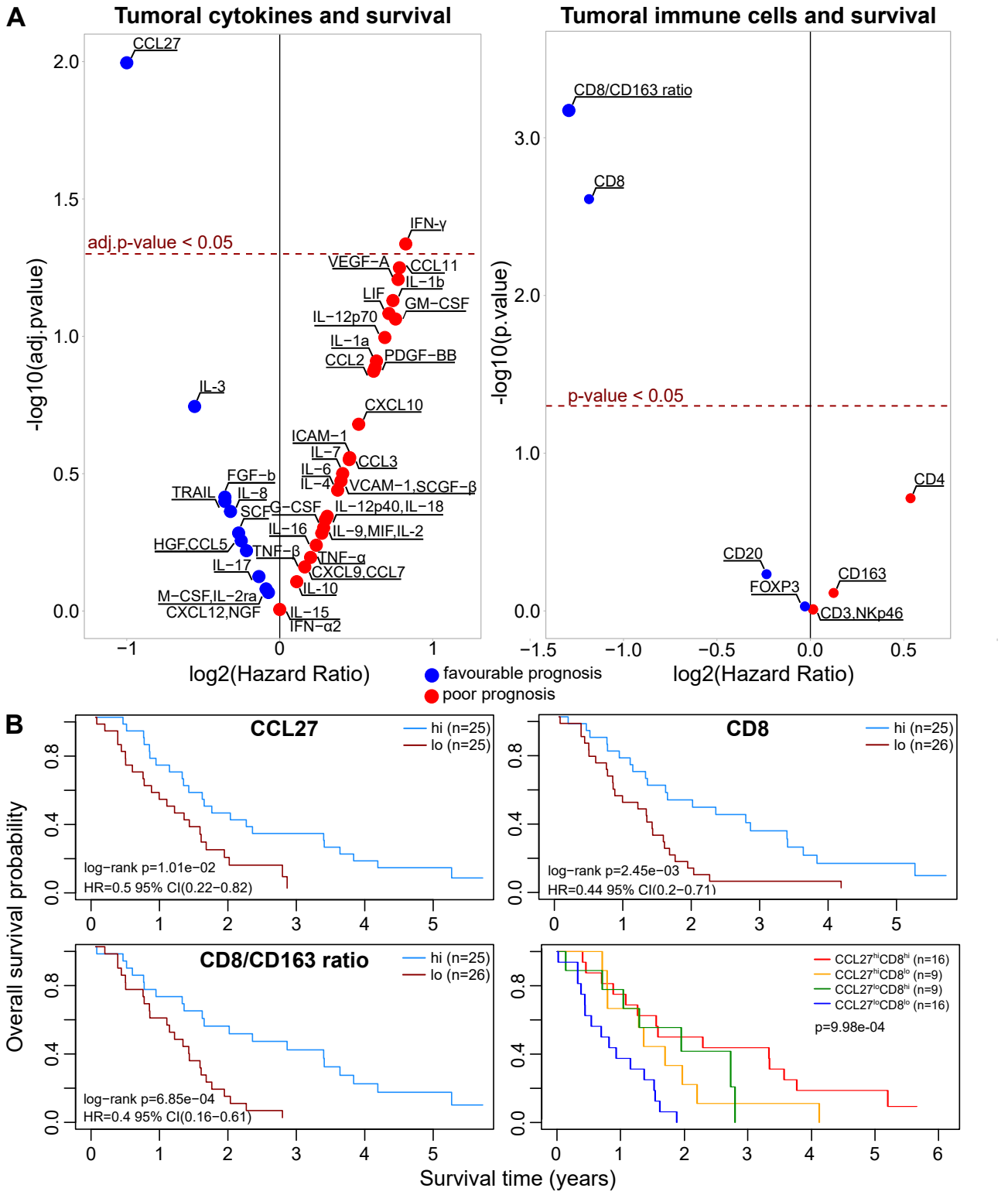

Figure 1 Intratumoral CCL27 expression is associated with improved overall survival
(A) Volcano plot of statistical significance (y-axis) against log2(Hazard Ratio) (x-axis) for cytokines (left) and immune cells (right) showing favorable and poor prognostic markers.
(B) Kaplan-Meier survival plots of patients with high (hi) versus low (lo) concentration of CCL27 (n=25/n=25), hi versus lo density of CD8+ T cells (n=25/n=26), hi versus lo CD8+/CD168+ ratio (n=25/n=26) and the combination of CCL27 (hi or lo) and CD8+ T cells (hi or lo). The median cutpoints were determined to stratify patients into hi and lo.
Survival data were analyzed using the log-rank test.
See also Figure S1.

Figure 2

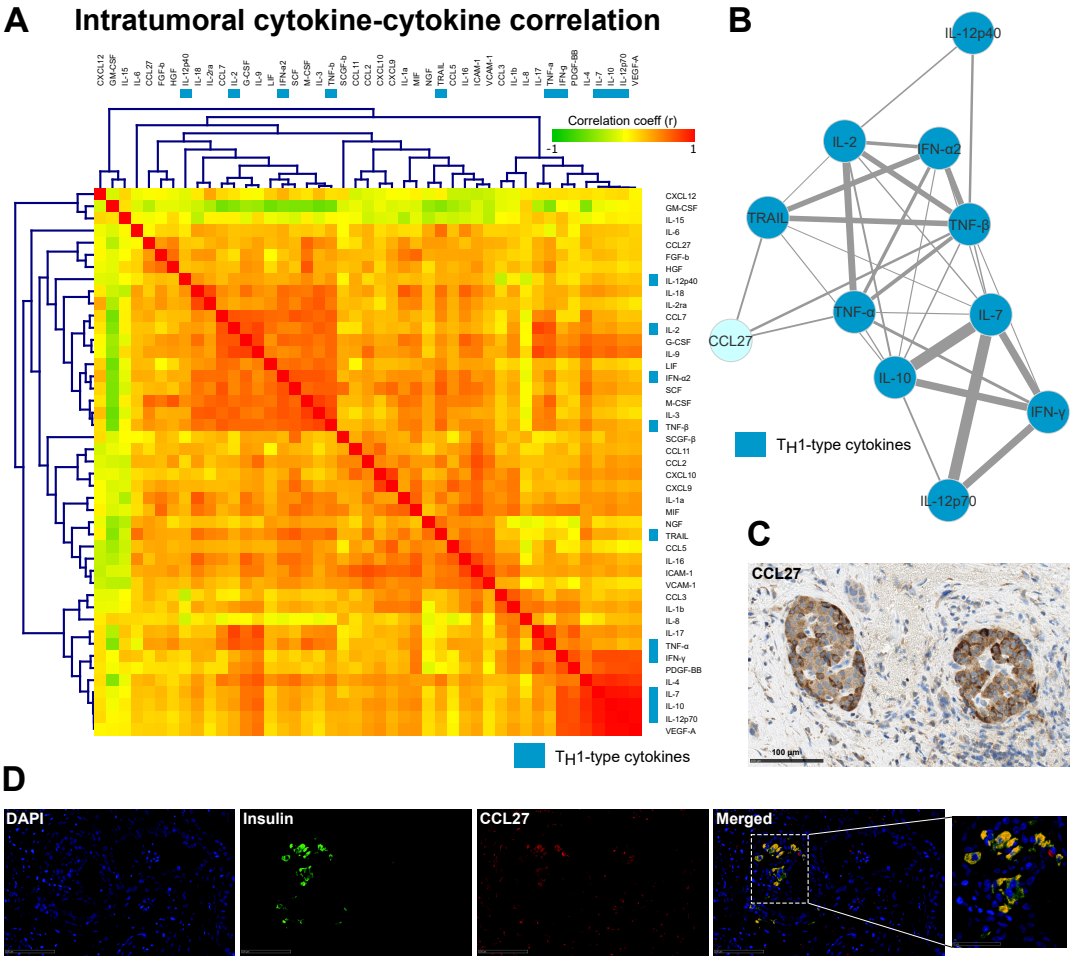

Figure 2 β-cells within Langerhans islets are the source of CCL27 and its expression is correlated with a TH1-type cytokine program

(A) Heatmap showing the intratumoral cytokine-cytokine correlation from human PDA tissue samples (n=48). TH1-type cytokines are indicated in blue.

(B) Network plot of intratumoral cytokine-cytokine correlations of TH1-type cytokines in human PDA tissue samples (n=48). The edge weights of the network are based on the Pearson correlation coefficient between cytokine-cytokine ($r \geq 0$, $p<0.05$).

(C) Immunohistochemistry for CCL27 in a human PDA tissue sample. Scale bars, 100 μm.

(D) Immunofluorescence for CCL27 and insulin (β-cell marker) in a human PDA tissue sample. Scale bars, 100 μm

PDA= pancreatic ductal adenocarcinoma

Figure 3

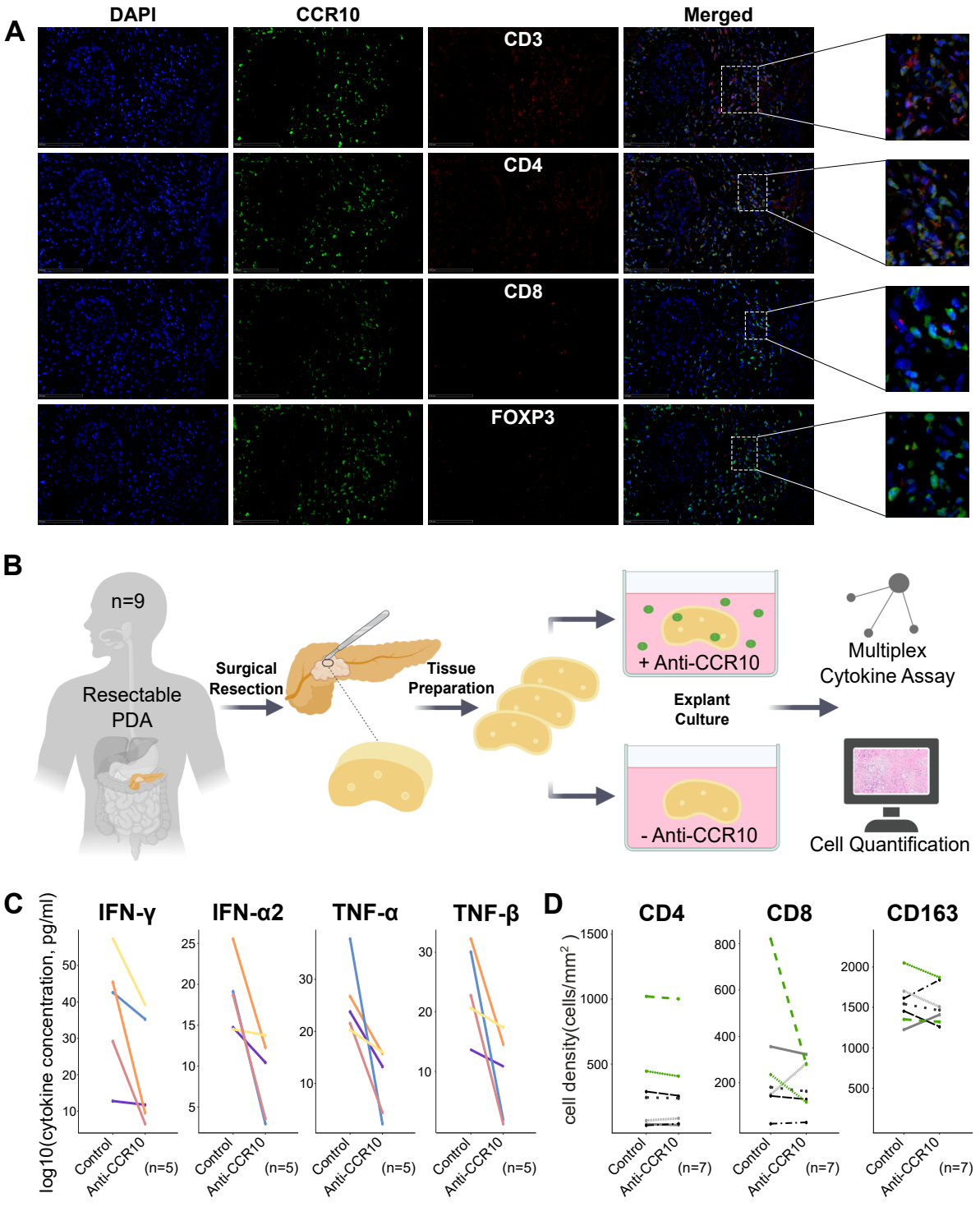

Figure 3 CCR10 is expressed on CD4+ FoxP3- T cells and selective inhibition of CCR10 abrogates the TH1-type cytokine profile

(A) Immunofluorescence of serial human PDA tissue samples as indicated. Scale bars, 100 µm.

(B) Schematic overview of workflow as indicated.

(C) Cytokine alterations within the explant model after 24 hr using human PDA tissue samples. Data from five different patients is presented before and after treatment with the small molecule inhibitor of CCR10 (Anti-CCR10).

(D) Alteration of the intratumoral CD4+, CD8+ and CD163+ immune cell infiltration within the explant model using human PDA tissue samples. Data from seven different patients is presented before and after treatment with the small molecule inhibitor of CCR10 (Anti-CCR10). The two tissues with the highest absolute number of intratumoral CD4+ cells are indicated in green.

PDA= pancreatic ductal adenocarcinoma

See also Figure S3.

Figure 4

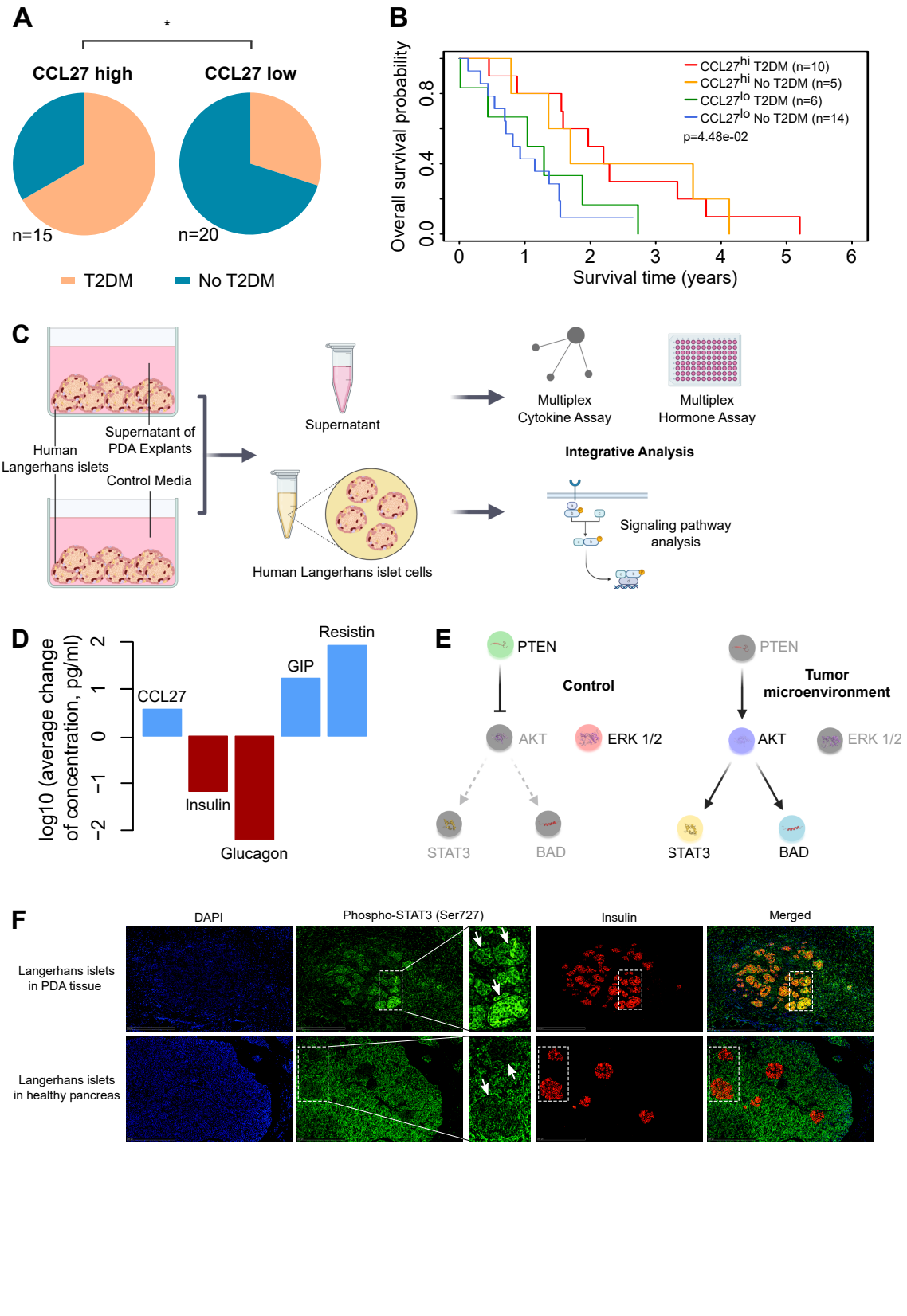
A
*
CCL27 high
CCL27 low
n=15
n=20
T2DM
No T2DM
B
Overall survival probability
0.0
0.4
0.8
0
1
2
3
4
5
6
Survival time (years)
CCL27hi T2DM (n=10)
CCL27hi No T2DM (n=5)
CCL27lo T2DM (n=6)
CCL27lo No T2DM (n=14)
p=4.48e-02
C
Human Langerhans islets
Supernatant of PDA Explants
Control Media
Supernatant
Human Langerhans islet cells
Multiplex Cytokine Assay
Multiplex Hormone Assay
Integrative Analysis
Signaling pathway analysis
D
log10 (average change of concentration, pg/ml)
2
1
0
−1
−2
CCL27
Insulin
Glucagon
GIP
Resistin
E
PTEN
Control
AKT
ERK 1/2
STAT3
BAD
PTEN
Tumor microenvironment
AKT
ERK 1/2
STAT3
BAD
F
DAPI
Phospho-STAT3 (Ser727)
Insulin
Merged
Langerhans islets in PDA tissue
Langerhans islets in healthy pancreas

Figure 4 Intratumoral Langerhans islet cells secrete CCL27 via STAT3 regulation and simultaneously downregulate insulin production

(A) Pie charts showing the distribution of PDA patients with diagnosis of diabetes prior to surgery. The patients were stratified into CCL27 high (hi) (n=15) and CCL27 low (lo) (n=20) group based on their intratumoral CCL27 concentration.

(B) Kaplan-Meier survival plot of patients based on combination of CCL27 (hi or lo) and T2DM (yes or no). The patients were stratified into CCL27 hi and CCL27 lo group based on their intratumoral CCL27 concentration. The data were analyzed using the log-rank test.

(C) Schematic overview of workflow as indicated.

(D) Alteration of indicated protein concentration expressed by human Langerhans islet cells after 48 hr culture in the supernatant of five different human PDA explants (representing five different human pancreatic tumor microenvironments). The expression profile was compared to human Langerhans islet cells cultured in control media for 48 hr.

(E) Schematic signaling effects of Langerhans islets cells in a pancreatic tumor microenvironment. Grey molecules are inactive and colored molecules are active.

(F) Immunofluorescence of human PDA tissue and healthy pancreas tissue as indicated. Arrows indicate Langerhans islets. Scale bars, 500 μm.

T2DM= type 2 diabetes mellitus

PDA= pancreatic ductal adenocarcinoma

*p≤0.05.

See also Figure S4.

Figure 5

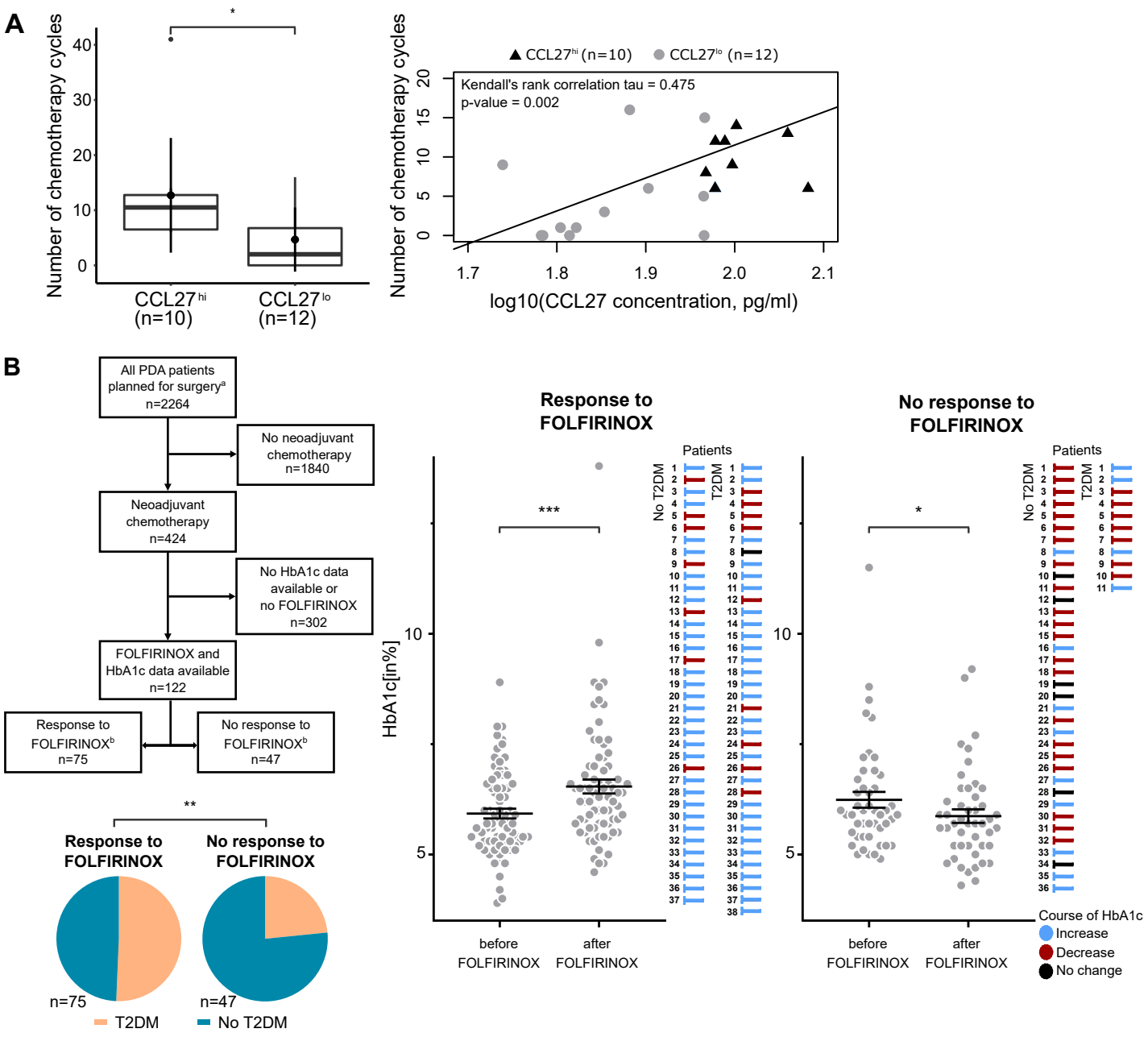
A
Number of chemotherapy cycles
CCL27hi (n=10)
CCL27lo (n=12)
Kendall's rank correlation tau = 0.475
p-value = 0.002
log10(CCL27 concentration, pg/ml)
B
All PDA patients planned for surgery[a] n=2264
No neoadjuvant chemotherapy n=1840
Neoadjuvant chemotherapy n=424
No HbA1c data available or no FOLFIRINOX n=302
FOLFIRINOX and HbA1c data available n=122
Response to FOLFIRINOX[b] n=75
No response to FOLFIRINOX[b] n=47
Response to FOLFIRINOX
No response to FOLFIRINOX
n=75
n=47
T2DM
No T2DM
HbA1c[in%]
Patients
before FOLFIRINOX
after FOLFIRINOX
Course of HbA1c
Increase
Decrease
No change
C
Diagnosis of PDA and T2DM
Start of chemotherapy
HbA1c level: 7,9%
Worsened glycemic control
End of chemotherapy
HbA1c level: 8,7%
9 cycles of chemotherapy with FOLFIRINOX
month(s)
Exploratory surgery (irresectable)
CCL27 expresssion: 127.17 pg/ml
Clinical Improvement
Increased CCL27 expression
Resectable after response to FOLFIRINOX (pancreatoduodenectomy)
CCL27 expresssion: 147.34 pg/ml

Figure 5 T2DM and dynamic of HbA1c levels are markers for response to neoadjuvant chemotherapy

(A) Comparison between CCL27 high (hi) and CCL27 low (lo) group based on the number of chemotherapy cycles. Standard treatment regimen was FOLFIRINOX as neoadjuvant chemotherapy. The patients were stratified into CCL27 hi and CCL27 lo group based on their intratumoral CCL27 concentration (left). Correlation analysis showing the association of CCL27 concentrations with number of chemotherapy cycles. The analysis was performed using the Kendall rank correlation (right).

(B) Retrospective analysis performed on a total of 2264 patients. HbA1c levels (before and after FOLFIRINOX) were available from 122 patients who were treated with neoadjuvant chemotherapy. The pie charts are showing the distribution of PDA patients with diagnosis of T2DM at the beginning of neoadjuvant chemotherapy with FOLFIRINOX. The patients were stratified into Response to FOLFIRINOX (n=75) and No response to FOLFIRINOX (n=47). Comparison of HbA1c levels before and after FOLFIRINOX treatment in responders and non-responders. The course of HbA1c levels of individual patients are described as indicated (blue=increase, red=decrease, black=no change).

(C) Timeline describing the case of a patient as indicated.

*p≤0.05, **p≤0.005, ***p≤0.0001.

a All PDA patients planned for pancreatoduodenectomy from 2016-2020 in the University Hospital Heidelberg were included.

b Response to FOLFIRINOX was assumed when the tumor was resectable. No response to FOLFIRNOX was assumed when the tumor remained irresectable.

Data are represented as mean ± SEM and compared by two-sided Student’s t test.

PDA= pancreatic ductal adenocarcinoma

T2DM= type 2 diabetes mellitus

FOLFIRINOX= fluorouracil, leucovorin, irinotecan and oxaliplatin

See also Figure S5.